Journal of The Electrochemical Society

The Electrochemical Society
Advancing solid state & electrochemical science & technology

Combinatorial Investigations of Ni-Si Negative Electrode Materials for Li-Ion Batteries

To cite this article: Zhijia Du *et al* 2015 *J. Electrochem. Soc.* **162** A1858

View the article online for updates and enhancements.

This content was downloaded from IP address 134.190.164.6 on 09/02/2023 at 13:46

Journal of The Electrochemical Society, **162** (9) A1858-A1863 (2015)
0013-4651/2015/162(9)/A1858/6/$33.00 © The Electrochemical Society

Combinatorial Investigations of Ni-Si Negative Electrode Materials for Li-Ion Batteries

Zhijia Du,[a,*] T. D. Hatchard,[b,] R. A. Dunlap,[a,c,d] and M. N. Obrovac[a,b,c,**,z]**

[a]*Department of Physics and Atmospheric Science, Dalhousie University, Halifax, Nova Scotia B3H 4R2, Canada*
[b]*Department of Chemistry, Dalhousie University, Halifax, Nova Scotia B3H 4R2, Canada*
[c]*Institute for Research in Materials, Dalhousie University, Halifax, Nova Scotia B3H 4R2, Canada*
[d]*College of Sustainability, Dalhousie University, Halifax, Nova Scotia B3H 4R2, Canada*

Sputtered thin films in the Ni-Si system ($0 \leq x \leq 0.65$ in Ni_xSi_{1-x}) were studied for use as anode materials in Li-ion cells. All compositions were found to be amorphous. The Ni in Ni-Si films was found to suppress the lithiation voltage, resulting in a reduction in capacity. The delithiation voltage was not affected. No capacity was observed when Ni content was more than 50 at% because at this composition the lithiation voltage was suppressed to 0 V. In contrast to previous models of capacity in transition metal-Si films, all Si atoms were found to be active in Ni-Si films at all compositions. Capacity reduction is only caused by a suppression of the Si lithiation voltage. We attribute this voltage suppression to internal stress in the thin film during lithiation from the presence of Ni.
© 2015 The Electrochemical Society. [DOI: 10.1149/2.0731509jes] All rights reserved.

Manuscript submitted April 21, 2015; revised manuscript received June 17, 2015. Published June 30, 2015.

Si containing materials are promising candidates as anode materials for lithium ion batteries. This is owing to the high theoretical capacity of Si (2194 Ah/L, compared to 764 Ah/L for graphite).[1] Pure Si, however, suffers from severe volume expansion (280% in the fully lithiated state) during the lithiation/delithiation process.[2] High internal stress in the electrode can lead to particle cracking, poor electrical contact and thus poor cycling stability. The use of active/inactive alloys is an efficient way to reduce volume expansion and improve cycling performance.[1,3] In this approach, the volume expansion of Si can be diluted by the presence of inactive components, resulting in the maximum energy density at a given volume expansion.[1]

Binary Si-TM alloys (TM referring to a transition metal which is inactive with lithium) have been extensively studied for many years as active/inactive materials. Transition metals in alloys can facilitate the production of an amorphous/nanocrystalline state, reduce the overall volume change by limiting specific capacity, and suppressing the formation of $Li_{15}Si_4$ during lithiation.[4–6] However, the reversible capacity of Si-TM binary alloys varies greatly in the literature.[5–13] Specifically for the Ni-Si system, some researchers have found that Ni-Si intermetallic compounds have considerable activity toward lithium. Wang et al. reported that ball-milled NiSi has a capacity of 1180 mAh/g.[7,8] This capacity is close to the value of 1158 mAh/g corresponding to the mechanism in which Li reacts with all Si in NiSi to produce $Li_{15}Si_4$ and Ni. Zhou et al. synthesized a thin film of the NiSi intermetallic phase by laser deposition.[9] Electrochemical studies showed that the Si in this phase was fully active, resulting in a capacity of 1220 mAh/g and that this reaction was fully reversible.[9] Liu et al. reported an in-situ X-ray diffraction (XRD) study of a NiSi-Si composite made by mechanical milling.[10] They concluded that NiSi has a reversible capacity of 579 mAh/g with Li_xSi and inactive Ni_2Si being formed during lithiation.[10]

There are also many reports that Ni-Si intermetallic compounds are inactive toward Li. Netz and Huggins reported that $NiSi_2$ made by an undisclosed method had limited activity toward Li, with a capacity of only 198 mAh/g.[11] Later, Park et al. reported that the XRD peaks of $NiSi_2$ made by arc-melting and subsequent high-energy mechanical milling remained unchanged when a Si/Ni alloy-graphite composite electrode was cycled between 5 mV and 1.5 V.[12] Park et al. then reported the use of inactive NiSi and $NiSi_2$ to dilute the volume expansion of active Si in a Ni–Si alloy–graphite composite with 800 mAh/g capacity and good cycleability.[13]

More general studies of combinatorially sputtered amorphous/nanocrystalline Si-TM thin film alloys with TM = Fe, Mn, Cr+Ni, Co, by Fleischauer et al. have suggested that sputtered Si-TM films are composed of a mixture of active amorphous Si and inactive transition-metal silicides.[5,6] By using an effective heat of formation model, it was predicted that FeSi, MnSi, NiSi and $CoSi_2$ were the inactive phases formed in Si-TM thin films. This model correlated well with the trend in the alloy capacity in lithium-ion cells as a function of film composition.[6] However, Ni-Si differs from the Mn-Si, Fe-Si, Co-Si or Cr-Si alloys studied previously because it forms an equilibrium ternary phase with Li, as shown in the Li-Ni-Si phase diagram in Figure 1. According to the International Centre for Diffraction Data (ICDD),[16] the Fe-Si, Co-Si, Cr-Si and Mn-Si alloy systems do not have any ternary phases with Li. Therefore, the electrochemical behavior of the Ni-Si system with lithium may be different.

Previous studies of active/inactive alloys have not considered the effect of the internal stress induced by the presence of the inactive phase as the active phase expands during lithiation on the voltage curve of Si. However, it is well known that stress-potential coupling occurs during the lithiation of Si thin films from stress induced by the fixed substrate.[17] This effect is significant. Compressive stress occurs during volume expansion (lithiation) and results in voltage depression, while tensile stress occurs during delithiation and results in voltage elevation. Some of the tensile stress that occurs during delithiation may be relieved by cracks formation.[17] The amount of shift in the voltage curve of thin Si films due to stress induced by the substrate can be as much as 200 mV and results in significant changes in Si electrochemistry. We have found that the depression of the lithiation voltage curve by stress in Si thin films is sufficient to eliminate the formation of $Li_{15}Si_4$.[18] It is likely that stresses due to an inactive phase in an alloy particle could be significantly larger than that induced in a thin film by a substrate. Therefore this effect should be considered when studying active/inactive alloys.

In the present study, Ni_xSi_{1-x} thin film libraries were synthesized by combinatorial sputtering with x spanning the range from 0 to 0.65. A structural and compositional analysis of the films and the effect of composition on their electrochemical behavior are discussed. It was found that the capacity of Ni_xSi_{1-x} thin film could not be explained by the lithiation mechanisms proposed in any of the previous studies of Si-TM films. Instead, it was found that increasing Ni content suppressed the average lithiation voltage, resulting in capacity reduction. Surprisingly, the delithiation voltage remained unchanged. This behavior could be explained in terms of stress-induced voltage changes, rather than Si inactivation. These results suggest that other Si-TM thin film systems should be more carefully re-investigated for voltage suppression caused by inactive phases as well as by substrates.

Experimental

Thin film libraries of Ni-Si were fabricated using a modified Corona Vacuum System V3-T sputtering system as described before.[19]

*Electrochemical Society Student Member.
**Electrochemical Society Active Member.
[z]E-mail: mnobrovac@dal.ca

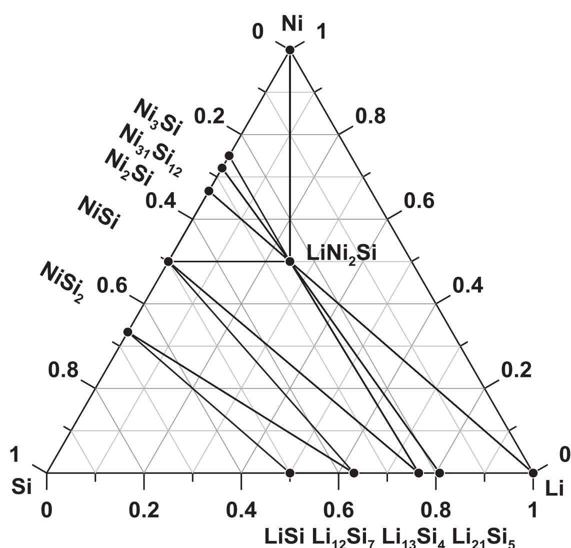

Figure 1. Li-Ni-Si ternary phase diagram at 0 K as predicted by the Materials Project.[14,15]

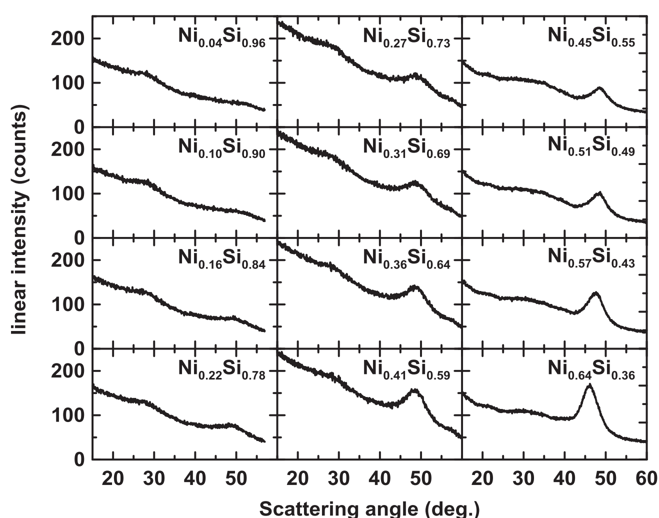

Figure 2. XRD spectra of Ni_xSi_{1-x} thin films with selected compositions deposited on a Si (100) wafer.

The base pressure for sputtering was below 4×10^{-7} Torr. Ar gas flow maintained the pressure at 1.5 mTorr during sputtering. Si sputtering targets (99.9% purity, Pure Tech) were 50 mm diameter × 6 mm thick and Ni sputtering targets (99.5% purity, Aesar) were 50 mm diameter × 0.7 mm thick. In total, three Ni_xSi_{1-x} libraries denoted as lib1 ($0 \leq x \leq 0.28$), lib2 ($0.22 \leq x \leq 0.51$) and lib3 ($0.41 \leq x \leq 0.65$) were prepared using a constant mask for the Si target, a linear-out mask for one Ni target, and a constant mask for a second Ni target (for lib 2 and lib 3). The composition range of each library extended over a 76 mm wide sputtering track on the substrate.

Films were deposited on Cu foil discs with an area of 1.3 cm^2, a glass plate (2 cm × 10 cm) with Cu pre-sputtered on the surface and Si wafers. The Cu foil discs were punched from Cu foil (Furukawa Electric Co., Japan) which was previously roughened with Scotch-Brite (3 M Scotch-Brite General Purpose Scouring Pad 96) and cleaned with acetone. The position dependency of the mass was determined by the weighing of Cu discs before and after sputtering using a Sartorius SE-2 microbalance (±0.1 μg resolution). Composition data were collected using a JEOL 8200 microprobe from measurements of samples sputtered on Cu coated glass plates. XRD measurements of samples sputter deposited on Si wafers were made using a Bruker D-8 Discover diffractometer equipped with a Vantec-2000 area detector and a Cu target X-ray tube.

Cu foil discs with sputtered thin films were assembled in 2325-type coin cells with Li metal foil (99.9%, Sigma-Aldrich) counter electrodes. 1 M $LiPF_6$ (BASF) in a solution of ethylene carbonate, diethyl carbonate and monofluoroethylene carbonate (volume ratio 3:6:1, all from Novolyte Technologies) was used as electrolyte. Cell assembly was carried out in an Ar-filled glove box. Cells were galvanostatically cycled at 30.0 ± 0.1°C between 5 mV and 0.9 V with a Maccor Series 4000 Automated Test System. A rate of C/10 rate was used for the 1st cycle and a C/5 rate for the following cycles, with a C/20 trickle discharge during the lithiation half-cycle. To accurately determine cycling rates, currents were initially calculated by assuming all the Si in the alloys was active and trial cells were made to cycle at these theoretical rates. Then, cells were re-made and cycled using currents calculated from the measured capacities of the trial cells. The equilibrium potentials of $Ni_{0.07}Si_{0.93}$ and $Ni_{0.23}Si_{0.77}$ thin films during discharge/charge were obtained by the galvanostatic intermittent titration technique (GITT). Current pulses at 0.1C were applied for 1 h, followed by a 10 h relaxation process.

Results

Three libraries of Ni_xSi_{1-x} thin films were sputtered with some overlap of composition. The compositions of the libraries were lib 1 ($0 \leq x \leq 0.28$), lib2 ($0.22 \leq x \leq 0.51$) and lib3 ($0.41 \leq x \leq 0.65$), as determined by microprobe analysis. Selected XRD patterns of thin films are shown in Figure 2. All the patterns have two broad diffraction peaks at around 28° and 49°, indicating the amorphous nature of sputtered thin films. With the increase of Ni content, the intensity of the peak at 49° increases and its position shifts slightly to lower angle. However, the exact identity of the two peaks is difficult to determine because of their broad nature. Si (pdf No. 00-027-1402), Ni (pdf No. 00-004-0850), Ni_2Si (pdf No. 00-048-1339), $NiSi_2$ (pdf No. 96-900-9025), Ni_3Si_2 (pdf No. 00-089-2906) and NiSi (pdf No. 00-085-0901) all have strong diffraction peaks from 45° to 50°.[16]

Figure 3 shows voltage curves of selected Ni_xSi_{1-x} thin films for the first 3 cycles. All the curves have sloping plateaus which are characteristic of amorphous Si-based alloys, in accordance with XRD results. The voltage curve of $Ni_{0.04}Si_{0.96}$ thin film is identical to that previously reported for amorphous Si with two distinct sloping plateaus.[20] With increasing x (Ni content), the cell polarization increases, and the low

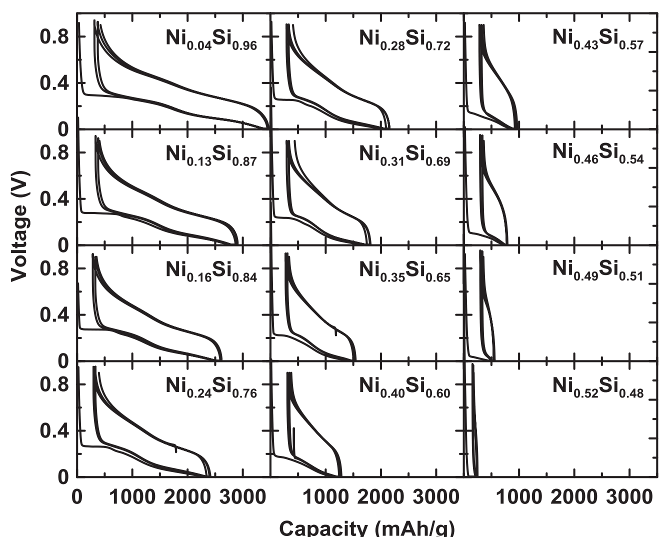

Figure 3. Voltage versus capacity curves of thin films with selected compositions.

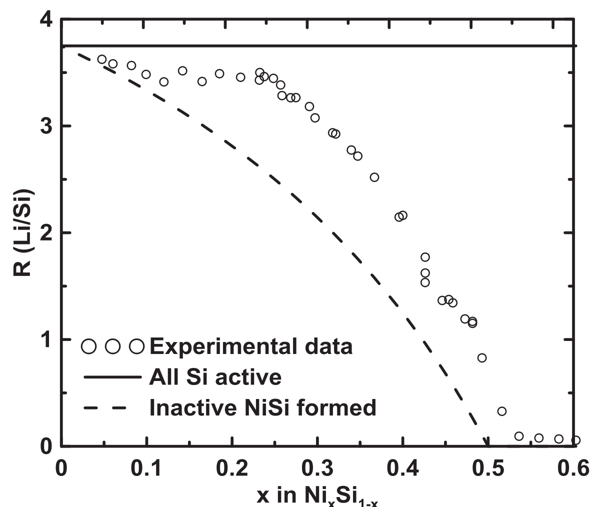

Figure 4. Li/Si atomic ratio calculated from the 1st reversible capacity versus composition.

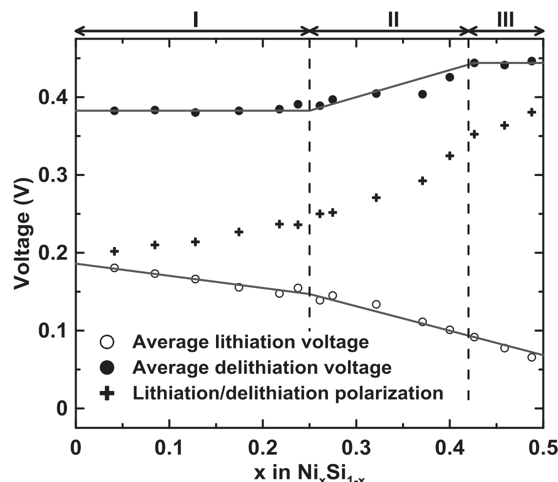

Figure 5. Average lithiation voltage, average delithiation voltage and polarization versus composition.

voltage lithiation plateau becomes relatively shorter and disappears when x is above 0.4. With further increases in x, the capacity decreases further. No obvious capacity can be observed when x is greater than 0.5. The irreversible capacity changes little with Ni content.

To examine these trends, the amount of Li inserted into the alloys was calculated from the 1st delithiation capacity since the absolute irreversible capacity remains nearly unchanged with varying Ni content. From this value, the Li/Si atomic ratio at full lithiation (defined here as R) was plotted versus composition in Figure 4. The value of R for $Ni_{0.04}Si_{0.96}$ is 3.624, slightly lower than the theoretical value of R = 3.75 (if all Si forms $Li_{15}Si_4$). This is consistent with previous reports of sputtered Si thin films that exhibit slightly lower capacity than the theoretical 3579 mAh/g.[21] This might be due to the absence of $Li_{15}Si_4$ formation and/or active material loss from particle fracture. Therefore, we believe that all the Si is active in the $Ni_{0.04}Si_{0.96}$ film.

As x in Ni_xSi_{1-x} increases from 0 to 0.25 in Figure 4, the value of R remains relatively constant, indicating that all the Si remains active at these compositions. The R value then decreases when x increases above 0.25. This would seem to indicate that some Si is becoming inactivated in these high Ni content films. It will be shown below that this is not the case. According to the model proposed by Fleischauer et al.,[6] the inactive phase formed in a sputtered Ni-Si film should be NiSi. Figure 4 also shows the R value plotted as a function of Ni content assuming that a Si/NiSi active/inactive alloy is formed, according to Fleischauer's model. This curve does not fit the observed data well. In fact, no Si/Ni_ySi active/inactive alloy combination can explain the trend in R shown in Figure 4.

Figure 5 shows the 2nd lithiation average voltage and first delithiation average voltage plotted as a function of x in Ni_xSi_{1-x}. Also shown in the figure is the total average cell polarization. The figure is separated into three regions. For thin films with $x \leq 0.25$ (Region I), the average lithiation voltage decreases with increasing x, while the average delithiation voltage maintains unchanged. This phenomenon has been recently reported by MacEachern et al. for Fe-Si-Zn alloys and was believed to be the reason why transition metal can suppress the formation of $Li_{15}Si_4$ during lithiation process.[4] As x increases into Region II there is an inflection point in both the average lithiation and delithiation voltages at x = 0.25, the average lithiation voltage is suppressed with a more negative slope, and the average delithiation voltage begins to increase. Interestingly, according to Figure 4, there is also an inflection point in R at x = 0.25, as discussed above. Therefore, it is likely that R and average lithiation/delithiation voltages are related. A third region is also apparent in Figure 5 for x above about 0.4. In Region III the delithiation voltage remains constant, while the average lithiation voltage continues to decrease with the increase of x. The significance of each of these regions will be discussed below.

Figure 6 shows the differential capacity curves derived from the voltage curves. The plots are grouped in columns according to the three regions shown in Figure 5. Two broad peaks during lithiation (denoted as peak A and B) and two corresponding peaks during delithiation (denoted as peak A′ and B′) can be clearly observed for the $Ni_{0.04}Si_{0.96}$ thin film. As x increases in Region I, the two lithiation peaks shift to less positive voltages with increasing Ni content, while the delithiation peaks show little change either in position or area. It is interesting that although peak B appears to be truncated at low voltages and high Ni content in Region I, the value of R remains unchanged for these compositions, as shown in Figure 4, and the peak B′ also does not change. This can be attributed to the constant current constant voltage (CCCV) mode of cycling. Although capacity is lost during the CC portion of the lithiation corresponding to the area truncated from the B peak in the differential capacity, this capacity can be accessed during the CV portion of the lithiation, during which time the discharge trickle current can fully lithiate thin films. The CV portion of the capacity is not visible in the differential capacity curve. The net result is that in Region I increasing Ni content in the thin films causes the suppression

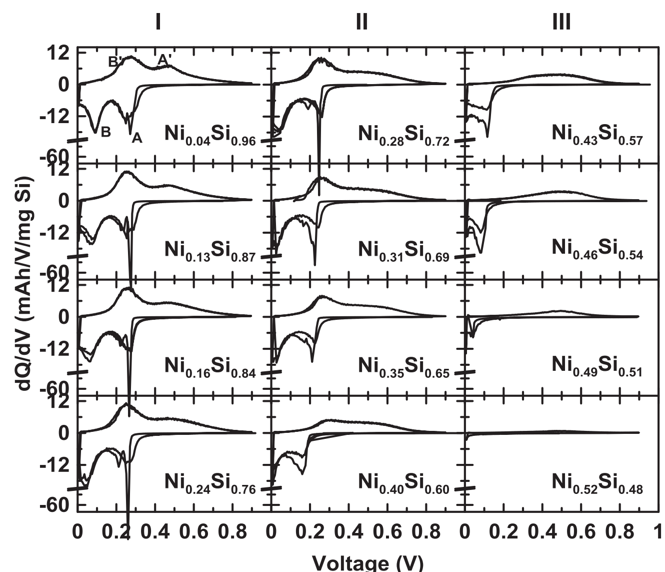

Figure 6. Differential capacity curves for cells shown in Figure 3.

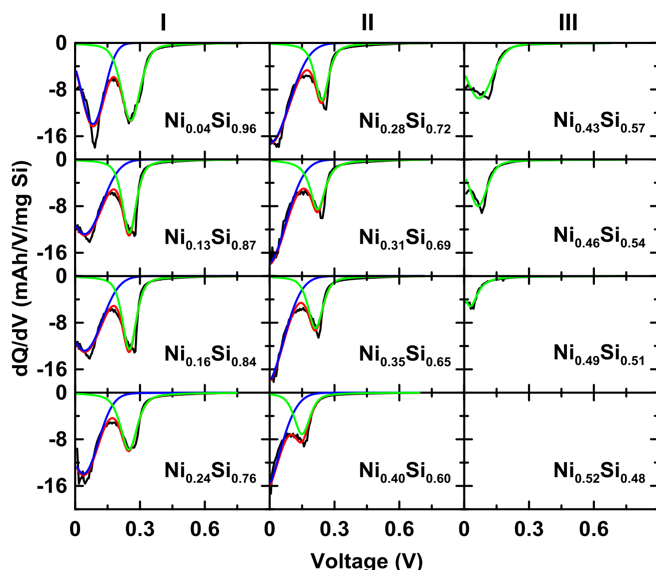

Figure 7. Pseudo-Voigt profiles fitting of two differential capacity curve peaks during lithiation of 2nd cycle.

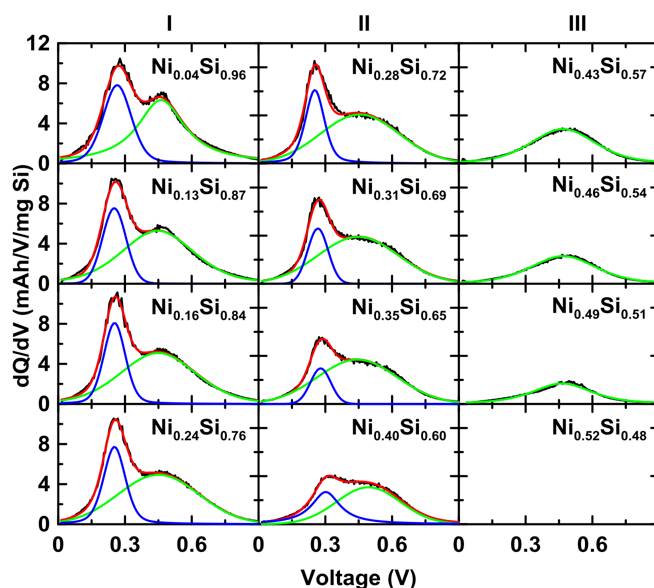

Figure 8. Pseudo-Voigt profiles fitting of two differential capacity curve peaks during delithiation of 1st cycle.

of the average lithiation voltage, while the average delithiation voltage and R value remain constant, as was observed in Figures 4 and 5.

In Region II, as x increases from 0.25 to 0.4, the A′ and B′ peak positions remain unchanged, while the two lithiation peaks shift to even less positive values and the B peak becomes truncated past the peak minimum. The capacity associated with the portion of this peak that now resides below 5 mV can no longer be accessed at low currents during the CV portion of the lithiation half-cycle. As a result the average lithiation voltage decreases at a faster rate as x increases in Region II, as is apparent in Figure 5. The loss in capacity of the B peak also causes the B′ peak area to decrease in area. As x increases to above 0.4 at the upper limit of Region II, the lithiation voltage shifts to such negative values that peak B disappears, causing the corresponding B′ peak to also disappear. However, the capacity of peak A is still fully accessed throughout Region II and, therefore, the capacity of peak A′ also remains unchanged. Since the B′ peak area decreases and the A′ peak area remains unchanged with increasing Ni content in Region II, the net result will be an increase in the average delithiation voltage and a decrease in R value in Region II, as is shown in Figure 4 and 5.

As x increases further, into Region III, the lithiation voltage continues to shift to negative values and peak A commences to truncate at zero volts. This causes a reduction in the corresponding delithiation peak A′. However the voltage of peak A′ remains unchanged, as will be shown below. The net result is that as the Ni content is increased in Region III, the value of R and the lithiation voltage continue to decrease, while the delithiation voltage remains constant, as is apparent in Figures 4 and 5.

The above analysis has shown that all the features in Figures 4 and 5 can be explained in terms of a negative shift in the lithiation voltage of Si-Ni alloys as the Ni content is increased, coupled with the CCCV cycling method employed during the lithiation half-cycle. To quantify these changes, the differential capacity curves were fit using pseudo-Voigt peak profiles, as shown in Figure 7 and 8. Here pseudo-Voigt peak profiles were used as an approximation, since differential capacity peaks do not necessarily have this shape, and furthermore become distorted at high Ni contents. Figure 9 shows the positions of peaks A and B according to the fit. The peaks shift slowly to lower voltage as x is increased to about $x = 0.25$. Beyond this point the peaks rapidly shift to more negative voltages. The fitted delithiation peak B′ and A′ voltages are plotted in Figure 10. In contrast to the lithiation peaks, the A′ and B′ peaks do not change with Ni content. At Ni contents higher than $x = 0.3$, the B′ peak appears to shift to higher voltages. However, the B′ peak is very small at these compositions and

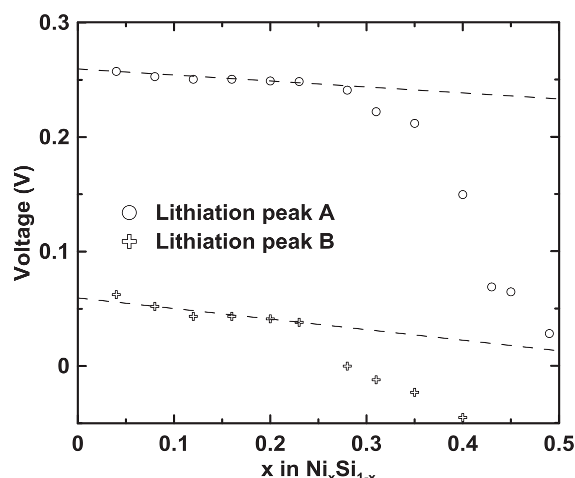

Figure 9. Lithiation Peak A and B voltages versus composition from fitting results in Figure 7.

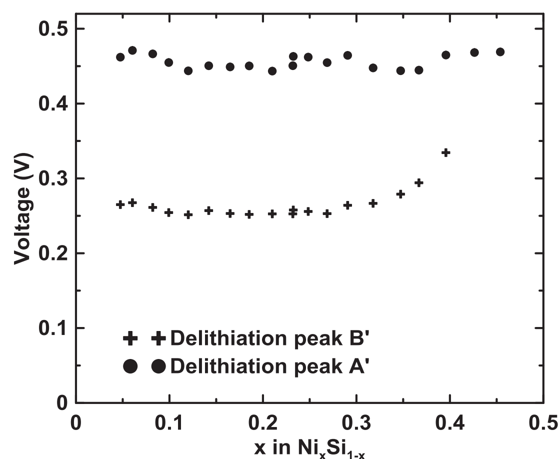

Figure 10. Delithiation Peak B′ and A′ voltages versus composition from fitting results in Figure 8.

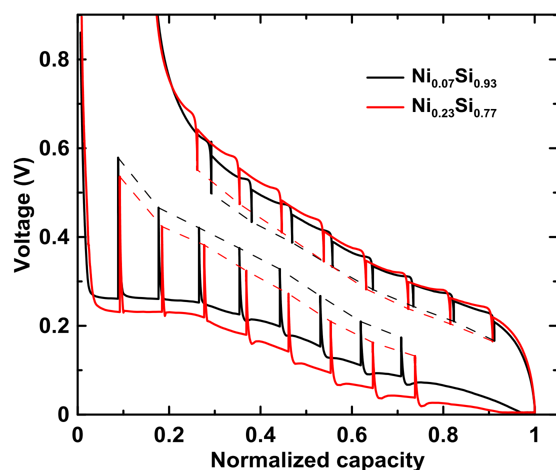

Figure 11. Open-circuit potential after ten-hour relaxation during lithiation and delithiation for thin films $Ni_{0.07}Si_{0.93}$ and $Ni_{0.23}Si_{0.77}$ with normalized capacity. Dashed lines connecting relaxation voltages are added as a guide to the eye.

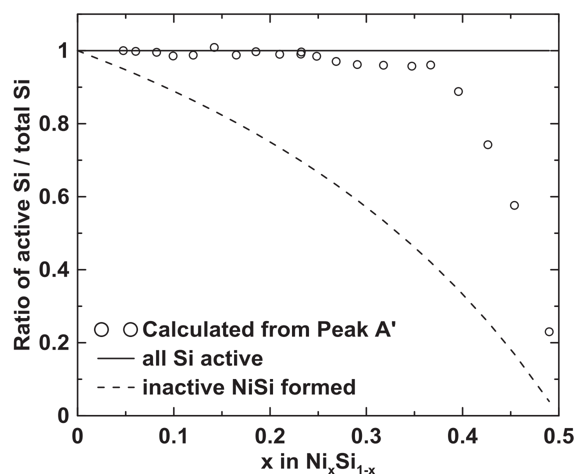

Figure 12. Active Si ratio calculated from the fitting result of delithiation peak A′ versus composition.

this apparent shift is likely due to error associated with convoluting this small peak from the large and broad A′ peak.

Figure 11 shows the GITT voltage curve of two Ni-Si thin films with different compositions. Apparently, the open-circuit potential at the same state of charge during lithiation after relaxation is lower than that during delithiation, as reported and explained before.[22–24] During discharge, the relaxed voltage is lower when the film has a higher Ni content. However, the relaxed voltage during charge shows little dependence on Ni content. This phenomenon may originate from internal stress in the film,[17,22] as will be discussed below. Thin films with higher content of Ni have higher internal stress and thus a lower cell potential in response. During charge, thin film fracture may release tension stress, leading to similar relaxed potential of both thin films.

Discussion

From the above analysis it is clear that the addition of Ni to Si causes capacity reduction via a shift in the lithiation voltage curve toward lower voltages. No other changes in the features of the voltage curve were observed. One explanation for this effect is that the suppression of the voltage curve is caused by Ni taking part in the lithiation reaction. For instance, if present in a Ni-Si solid solution, Ni could modify the chemical potential of Si and hence the voltage curve. Ni can furthermore form ternary Li-Ni-Si phases. We consider this to be a possible explanation for the phenomena observed here. However, this explanation is difficult to reconcile with the observed Ni-Si voltage curves, since if Ni was taking part in the electrochemical reaction one would expect the delithiation voltage curve to be also modified from that of pure Si, but it is not.

If one accepts that the active phase in the Ni-Si films is pure Si, then since the Si A/A′ redox couple is fully accessible toward reversible lithiation for x up to about 0.40, these peaks should be a good indicator of how much active Si is present in the Ni-Si films. Figure 12 shows the percent active Si present in the Ni-Si films calculated on the basis of the capacity under peak A′. Here percent active Si was calculated as the capacity under peak A′ relative to the peak A′ of the nearly pure Si film ($Ni_{0.04}Si_{0.96}$), which was assumed to have all active Si. According to this model, for x less than about 0.4, all Si atoms are active to Li. For higher x, all Si atoms may still be active because part of the lithiation peak A becomes inaccessible to Li as shown in Figure 6, due to further voltage suppression by Ni atoms. Therefore, based on the analysis and fitting of differential capacity curves, all Si atoms in the Ni-Si films are accessible to lithiation/delithiation and the capacity decrease is the result of lithiation voltage suppression because of the presence of inactive Ni in the films. This presents a new model for the capacity reduction in Si-TM films than was suggested by Fleischauer et al. The model suggested by Fleischauer et al. does not explain the behavior observed here and is also shown in Figure 12 for comparison. Actually, the shift of the lithiation voltage can be clearly seen in Ref. 5. However, the dQ/dV curves in Ref. 5 are, in fact, cyclic voltammetry curves using a constant voltage sweep rate. This makes the voltage shift difficult to quantify. Therefore, other Si-TM thin films should be re-investigated for voltage suppression caused by inactive phases.

It remains to be answered how inactive Ni could induce a negative voltage shift of Si during lithiation, but not change the Si delithiation voltage curve. We speculate that this behavior could arise from internal stress in the Ni-Si films induced by inactive Ni during cycling. In such a Si/Ni active/inactive film there would be enormous internal stress during lithiation, since the active Si regions would expand, whereas the inactive Ni regions would not. Sethuraman et al. have studied the stress-potential coupling in Si thin films sputtered on Cu substrates.[17] During lithiation compressive stress induced by the Cu substrate was measured to be as high as 1.5 GPa and caused the voltage to be suppressed by about 100–125 mV/GPa. This compressive stress could be released by plastic deformation. During delithiation the magnitude of the induced tensile stress was much less than the compressive stress during lithiation. This is because tensile stresses can be relieved by crack formation.[17] Therefore, stress induced voltage would tend to cause suppression of the lithiation voltage curve, while the delithiation voltage curve would be less effected. In the sputtered Ni-Si system, dispersed Ni atoms may function similarly as the substrate in Si thin films, generating high mechanical stresses during volume expansion as illustrated in Figure 13. In addition, the presence of Ni atoms in Si thin film leads to solid solution strengthening, allowing the films to tolerate high internal stresses. We believe this is a good explanation of the large magnitude in lithiation voltage suppression caused at high Ni content in our Ni-Si thin films, while maintaining the two peaks in differential capacity that are characteristic of the Si voltage curve.

To quantify the amount of internal stress that could cause the observed shifts in voltage, the shift of peak A compared to that of $Ni_{0.04}Si_{0.96}$ is plotted as a function of Ni content in Figure 14. For $Ni_{0.19}Si_{0.81}$, the shift in the voltage of peak A is −23.9 mV, which means the internal stress increases by about 191–239 MPa using the voltage shift-stress relationship of 100–125 mV/GPa as reported by Sethuraman et al.[17] During delithiation, the voltage remains unchanged with increasing Ni content, due to the formation of cracks which releases the tensile stress, as explained above. At higher Ni contents, the magnitude of the induced voltage shift increases dramatically. For $Ni_{0.45}Si_{0.55}$ the voltage shift is −275 mV, corresponding to about 2.2–2.75 GPa. These internal stresses are higher than are

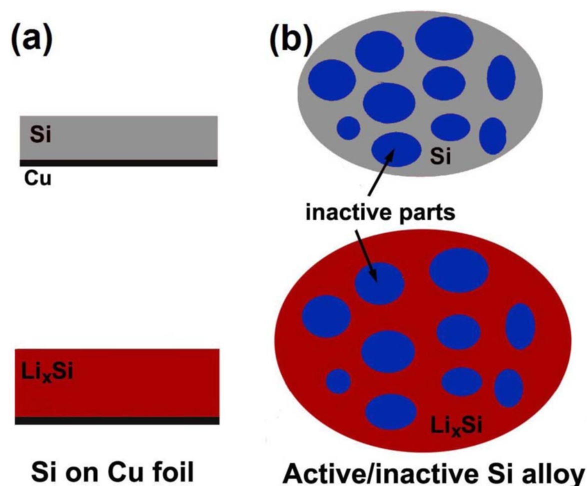

Figure 13. Illustration of (a) stress caused by Cu foil in Si thin film during lithiation and (b) stress caused by inactive parts in active/inactive Si alloys. The red color indicates the Li_xSi is under compression stress.

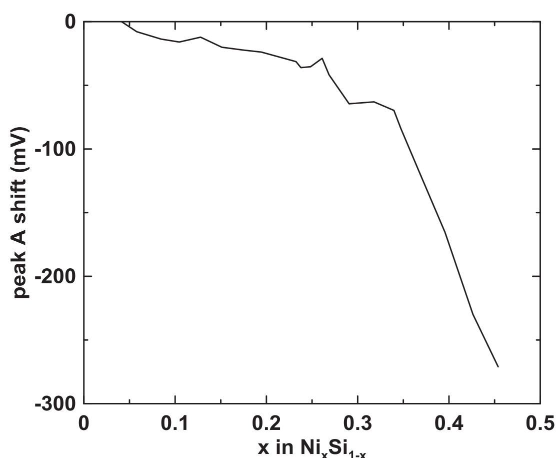

Figure 14. Voltage shift of peak A in differential capacity curves versus composition.

induced by a current collector (1.5 GPa),[17] since we speculate that they are being caused by an internal inactive phase, which may exert significantly more compressive stress on a nano-Si grain than a current collector could exert on a microns-thick Si film.

Conclusions

A large composition range of amorphous Ni_xSi_{1-x} thin films was sputtered and investigated as anode materials for Li-ion cells. The structure of all thin films showed amorphous characteristics. Capacity variation versus Ni content did not fit with any previous reports. The average lithiation voltage was found to decrease with the increase of x while average delithiation voltage maintained unchanged for x less than 0.25 and began to increase with the increase of x afterwards. Differential capacity analysis suggests that all Si atoms are active for all compositions in Ni_xSi_{1-x} and the decreased capacity with increasing Ni content is only caused by suppression of the Si lithiation voltage. This voltage suppression was attributed to internal stress-voltage coupling caused by the inactive Ni phase. This presents a new explanation for the capacity trend of Si-TM alloys, based on newly observed voltage behavior. We believe that other Si-TM alloys should be re-investigated in the context of the present results.

Acknowledgments

The authors acknowledge funding from NSERC and 3 M Canada, Co. under the auspices of the Industrial Research Chair program. We also acknowledge the support of the Canada Foundation for Innovation, the Atlantic Innovation Fund and other partners that fund the Facilities for Materials Characterization managed by the Institute for Research in Materials. ZD acknowledges financial support from the Killam Trusts.

References

1. M. N. Obrovac, L. Christensen, Dinh Ba Le, and J. R. Dahn, *J. Electrochem. Soc.*, **154**, A849 (2007).
2. M. N. Obrovac and L. Christensen, *Electrochem. Solid-State Lett.*, **7**, A93 (2004).
3. O. Mao, R. L. Turner, I. A. Courtney, B. D. Fredericksen, M. I. Buckett, L. J. Krause, and J. R. Dahn, *Electrochem. Solid-State Lett*, **2**, 3 (1999).
4. L. MacEachern, R. A. Dunlap, and M. N. Obrovac, *J. Electrochem. Soc.*, **162**, A229 (2015).
5. M. D. Fleischauer, J. M. Topple, and J. R. Dahn, *Electrochem. Solid-State Lett*, **8**(2), A137 (2005).
6. M D. Fleischauer, R. Mar, and J. R. Dahn, *J. Electrochem. Soc.*, **154**(3), A151 (2007).
7. G. Wang, L. Sun, D. Bradhurst, S. Zhong, S. Dou, and H. Liu, *J. Power Sources*, **88**(2), 278 (2000).
8. G. Wang, L. Sun, D. Bradhurst, S. Zhong, S. Dou, and H. Liu, *J. Alloys Compd.*, **306**(1-2), 249 (2000).
9. Y.-N. Zhou, W.-J. Li, H.-J. Chen, C. Liu, L. Zhang, and Z. Fu, *Electrochem. Comm.*, **13**(6), 546 (2011).
10. W.-R. Liu, N.-L. Wu, D.-T. Shieh, H.-C. Wu, M.-H. Yang, C. Korepp, J. O. Besenhard, and M. Winter, *J. Electrochem. Soc.*, **154**(2), A97 (2007).
11. A. Netz and R. A. Huggins, *Solid State Ionics*, **175**(1-4), 215 (2004).
12. M.-S. Park, Y.-J. Lee, S. Rajendran, M.-S. Song, H.-S. Kim, and J.-Y. Lee, *Electrochim. Acta*, **50**(28), 5561 (2005).
13. M.-S. Park, S. Rajendran, Y.-M. Kang, K.-S. Han, Y.-S. Han, and J.-Y. Lee, *J. Power Sources*, **158**(1), 650 (2006).
14. A. Jain, S. P. Ong, G. Hautier, W. Chen, W. D. Richards, S. Dacek, S. Cholia, D. Gunter, D. Skinner, G. Ceder, and K. A. Persson, *Appl. Phys. Lett. Mater.*, **1**, 011002 (2013).
15. S. P. Ong, W. D. Richards, A. Jain, G. Hautier, M. Kocher, S. Cholia, D. Gunter, V. L. Chevrier, K. A. Persson, and G. Ceder, *Comp. Mater. Sci.*, **68**, 314 (2013).
16. International Centre for Diffraction Data PDF-2, Release 2002.
17. V. A. Sethuraman, V. Srinivasan, A. F. Bower, and P. R. Guduru, *J. Electrochem. Soc.*, **157**(11), A1253 (2010).
18. D. S. M. Iaboni and M. N. Obrovac, in preparation.
19. J. R. Dahn, S. Trussler, T. D. Hatchard, A. Bonakdarpour, J. N. Meuller-Neuhaus, K. C. Hewitt, and M. Fleischauer, *Chem. Mater.*, **14**, 3519 (2002).
20. J. Li, A. Smith, R. J. Sanderson, T. D. Hatchard, R. A. Dunlap, and J. R. Dahn, *J. Electrochem. Soc.*, **156**, A283 (2009).
21. T. D. Hatchard and J. R. Dahn, *J. Electrochem. Soc.*, **151**, A838 (2004).
22. V. A. Sethuraman, V. Srinivasan, and J. Newman, *J. Electrochem. Soc.*, **160**(2) A394 (2013).
23. V. L. Chevrier and J. R. Dahn, *J. Electrochem. Soc.*, **157**(4), A392 (2010).
24. L. Baggetto, R. A. H. Niessen, F. Roozeboom, and P. H. L. Notten, *Adv. Funct. Mater.*, **18**, 1057 (2008).